Two-Higgs-Doublet Models and Enhanced Rates for a 125 GeV Higgs

Aleksandra Drozd[1,2],* Bohdan Grzadkowski[1],† John F. Gunion[2],‡ and Yun Jiang[2]§
(1) Faculty of Physics, University of Warsaw, 00-681 Warsaw, Poland and
(2) Department of Physics, University of California, Davis, CA 95616, USA

We examine the level of enhancement that can be achieved in the ZZ and $\gamma\gamma$ channels for a two-Higgs-doublet model Higgs boson (either the light h or the heavy H) with mass near 125 GeV after imposing all constraints from LEP data, B physics, precision electroweak data, vacuum stability, unitarity and perturbativity. The latter constraints restrict substantially the possibilities for enhancing the $gg \to h \to \gamma\gamma$ or $gg \to H \to \gamma\gamma$ signal relative to that for the SM Higgs, $h_{\rm SM}$. Further, we find that a significant enhancement of the $gg \to h \to \gamma\gamma$ or $gg \to H \to \gamma\gamma$ signal in Type II models is possible only if the $gg \to h \to ZZ$ or $gg \to H \to ZZ$ mode is even more enhanced, a situation disfavored by current data. In contrast, in the Type I model one can achieve enhanced rates in the $\gamma\gamma$ final state for the h while having the ZZ mode at or below the SM rate — the largest $[gg \to h \to \gamma\gamma]/[gg \to h_{\rm SM}\gamma\gamma]$ ratio found is of order ~ 1.3 when the two Higgs doublet vacuum expectation ratio is $\tan\beta = 4$ or 20 and the charged Higgs boson has its minimal LEP-allowed value of $m_{H^\pm} = 90$ GeV.

PACS numbers: 12.60.Fr, 14.80.Ec, 14.80.Fd
Keywords: Higgs physics, 2-Higgs-Doublet Model, LHC

arXiv:1211.3580v1 [hep-ph] 15 Nov 2012

I. INTRODUCTION

Data from the ATLAS and CMS collaborations [1, 2] provide an essentially 5σ signal for a Higgs-like resonance with mass of order 123–128 GeV. In the $\gamma\gamma$ final state, the ATLAS and CMS gluon fusion induced rates are significantly enhanced relative to the the Standard Model (SM) prediction. In the $gg \to h \to ZZ \to 4\ell$ channel, the ATLAS and CMS signals are not far from the SM expectation, with ATLAS showing a slight enhancement and CMS showing a slight suppression. In the $b\bar{b}$, $\tau^+\tau^-$ and $WW \to \ell\nu\ell\nu$ channels, the central value ATLAS rates are somewhat suppressed relative to the SM prediction but error bars are very large. The CMS signals in these latter channels are also somewhat suppressed and lie at least 1σ below the SM prediction — no signal being observed in the $\tau^+\tau^-$ channel. Meanwhile, the CDF and D0 experiments have announced new results [3] that support the ~ 125 GeV Higgs signal and suggest an enhancement relative to the SM of the W+Higgs with Higgs$\to b\bar{b}$ rate by a factor of 2 ± 0.6.

Enhancements with respect to the SM in the $\gamma\gamma$ channel are generically possible in two-Higgs-doublet models (2HDM) of Type-I and Type-II as explored in [4, 5]. However, these papers do not make clear what level of enhancement is possible after all constraints from B physics and LEP data (B/LEP), precision electroweak data, unitarity and perturbativity are imposed. In this paper, we impose all such constraints and determine the maximum possible enhancement. We employ a full 1-loop amplitude for Higgs$\to \gamma\gamma$ without neglecting any contributions from possible states in the loop. We examine correlations with other channels. We also consider cases of degenerate scalar masses at ~ 125 GeV [6].

*aleksandra.drozd@fuw.edu.pl
†bohdan.grzadkowski@fuw.edu.pl
‡jfgunion@ucdavis.edu
§yunjiang@ucdavis.edu

II. 2HDM MODELS

The general Higgs sector potential employed is

$$\begin{aligned}\mathcal{V} =& m_{11}^2 \Phi_1^\dagger \Phi_1 + m_{22}^2 \Phi_2^\dagger \Phi_2 - \left[m_{12}^2 \Phi_1^\dagger \Phi_2 + \text{h.c.} \right] \\ &+ \frac{1}{2}\lambda_1 \left(\Phi_1^\dagger \Phi_1 \right)^2 + \frac{1}{2}\lambda_2 \left(\Phi_2^\dagger \Phi_2 \right)^2 + \lambda_3 \left(\Phi_1^\dagger \Phi_1 \right) \left(\Phi_2^\dagger \Phi_2 \right) + \lambda_4 \left(\Phi_1^\dagger \Phi_2 \right) \left(\Phi_2^\dagger \Phi_1 \right) \\ &+ \left\{ \frac{1}{2}\lambda_5 \left(\Phi_1^\dagger \Phi_2 \right)^2 + \left[\lambda_6 \left(\Phi_1^\dagger \Phi_1 \right) + \lambda_7 \left(\Phi_2^\dagger \Phi_2 \right) \right] \left(\Phi_1^\dagger \Phi_2 \right) + \text{h.c.} \right\},\end{aligned} \tag{1}$$

where, to avoid explicit $\mathcal{CP}$ violation in the Higgs sector, all λ_i and m_{12}^2 are assumed to be real. We choose a basis in which

$$\langle \Phi_1 \rangle = \frac{v}{\sqrt{2}} \begin{pmatrix} 0 \\ \cos\beta \end{pmatrix} \qquad \langle \Phi_2 \rangle = \frac{v}{\sqrt{2}} \begin{pmatrix} 0 \\ e^{i\xi} \sin\beta \end{pmatrix},$$

where $v = (\sqrt{2} G_F)^{-1/2} \approx 246$ GeV. By convention $0 \leq \beta \leq \pi/2$ is chosen. For real parameters, the phase ξ could still be non-zero if the vacuum breaks $\mathcal{CP}$ spontaneously. We avoid parameter choices for which this happens and take $\xi = 0$. Then, we define

$$\Phi_a = \begin{pmatrix} \phi_a^+ \\ (v_a + \rho_a + i\eta_a)/\sqrt{2} \end{pmatrix} \qquad a = 1, 2 \tag{2}$$

with $v_1 = v\cos\beta$ and $v_2 = v\sin\beta$. The neutral Goldstone boson is $G^0 = \eta_1 \cos\beta + \eta_2 \sin\beta$ while the physical pseudoscalar state is

$$A = -\eta_1 \sin\beta + \eta_2 \cos\beta\,. \tag{3}$$

The physical scalars are:

$$h = -\rho_1 \sin\alpha + \rho_2 \cos\alpha, \quad H = \rho_1 \cos\alpha + \rho_2 \sin\alpha\,. \tag{4}$$

Without loss of generality, one can assume that the mixing angle α varies between $-\pi/2$ and $\pi/2$. We choose our independent variables to be $\tan\beta$ and $\sin\alpha$, which are single valued in the allowed ranges.

We adopt the code 2HDMC [7] for numerical calculations. A number of different input sets can be used in the 2HDMC context. We have chosen to use the "physical basis" in which the inputs are the physical Higgs masses $(m_H, m_h, m_A, m_{H^\pm})$, the vacuum expectation value ratio $(\tan\beta)$, and the $\mathcal{CP}$-even Higgs mixing angle, α, supplemented by m_{12}^2. The additional parameters λ_6 and λ_7 are assumed to be zero as a result of a Z_2 symmetry being imposed on the dim 4 operators under which $H_1 \to H_1$ and $H_2 \to -H_2$. $m_{12}^2 \neq 0$ is still allowed as a "soft" breaking of the Z_2 symmetry. With the above inputs, $\lambda_{1,2,3,4,5}$ as well as m_{11}^2 and m_{22}^2 are determined (the latter two via the minimization conditions for a minimum of the vacuum) [8].

In this paper we discuss the Type I and Type II 2HDM models, that are defined by the fermion coupling patterns as specified in Table I — for more details see [9].

	Type I			Type II		
Higgs	up quarks	down quarks	leptons	up quarks	down quarks	leptons
h	$\cos\alpha/\sin\beta$	$\cos\alpha/\sin\beta$	$\cos\alpha/\sin\beta$	$\cos\alpha/\sin\beta$	$-\sin\alpha/\cos\beta$	$-\sin\alpha/\cos\beta$
H	$\sin\alpha/\sin\beta$	$\sin\alpha/\sin\beta$	$\sin\alpha/\sin\beta$	$\sin\alpha/\sin\beta$	$\cos\alpha/\cos\beta$	$\cos\alpha/\cos\beta$
A	$\cot\beta$	$-\cot\beta$	$-\cot\beta$	$\cot\beta$	$\tan\beta$	$\tan\beta$

TABLE I: Fermionic couplings $C_{ff}^{h_i}$ normalized to their SM values for the Type I and Type II two-Higgs-doublet models.

III. SETUP OF THE ANALYSIS

The 2HDMC code implements precision electroweak constraints (denoted STU) and limits coming from requiring vacuum stability, unitarity and coupling-constant perturbativity (denoted jointly as SUP). The SUP constraints are

particularly crucial in limiting the level of enhancement of the $gg \to h \to \gamma\gamma$ channel, which is our main focus. For all our scans, we have supplemented the 2HDMC code by including the B/LEP constraints. For the LEP data we adopt upper limits on $\sigma(e^+e^- \to Z\,h/H)$ and $\sigma(e^+e^- \to A\,h/H)$ from [10] and [11], respectively. [1] Regarding B physics, the constraints imposed are those from BR($B_s \to X_s\gamma$), R_b, ΔM_{B_s}, ϵ_K, BR($B^+ \to \tau^+\nu_\tau$) and BR($B^+ \to D\tau^+\nu_\tau$). The most important implications of these results are to place a lower bound on $m_{H^\pm}$ as a function of $\tan\beta$ as shown in Fig. 15 of [12] in the case of the Type II model and to place a lower bound on $\tan\beta$ as a function of $m_{H^\pm}$ as shown in Fig. 18 of [12].

While looking for an enhancement of the signal in the $\gamma\gamma$ channel we also computed the extra Higgs-sector contributions to the anomalous magnetic moment of the muon, $a_\mu = (g_\mu - 2)/2$. Since the experimentally measured value, $a_\mu = (1165920.80 \pm 0.63) \times 10^{-9}$ [13], differs by $\sim 3\sigma$ from its SM value it is important to check correlations between $\delta a_\mu \equiv a_\mu - a_\mu^{SM}$ and the signal in the $\gamma\gamma$ channel. Given the B/LEP, STU and SUP constraints, it turns out that one-loop contributions within the 2HDM are small and negligible, and the leading contribution is that known as the Barr-Zee diagram [14] which emerges at the two-loop level. For completeness we include also sub-leading contributions, see [7]. Since the overall $\sim 3\sigma$ discrepancy between the experimental and theoretical SM values could still be due to fluctuations (the world average is based mainly on the E821 result [15] with uncertainties dominated by statistics) or underestimates of the theoretical uncertainties, we do not use the a_μ measurement as an experimental constraint on the models we discuss. However, in tables presented hereafter we do show (in the very last column in units of 10^{-11}) δa_μ, the judgment as to whether δa_μ is acceptable being left to the reader. In fact, for all parameter choices yielding an enhanced Higgs to two-photon rate the extra contributions to a_μ are very small and the a_μ discrepancy is not resolved.

Coupling constant perturbativity is defined as in 2HDMC by the requirement that all self-couplings among the Higgs-boson mass eigenstates be smaller than 4π. For the scenarios we consider, this becomes an important constraint on λ_1. By the vacuum stability constraint we mean positivity of the potential in all directions at asymptotically large field strength. Unitarity is the requirement that the multi-channel Higgs scattering matrix have a largest eigenvalue below the unitarity limit using the analysis of [16].

For an individual Higgs, denoted h_i (where $h_i = h, H, A$ are the choices) we compute the ratio of the gg or WW-fusion (VBF) induced Higgs cross section times the Higgs branching ratio to a given final state, X, relative to the corresponding value for the SM Higgs boson as follows:

$$R_{gg}^{h_i}(X) \equiv (C_{gg}^{h_i})^2 \, \frac{\mathrm{BR}(h_i \to X)}{\mathrm{BR}(h_{\mathrm{SM}} \to X)}, \quad R_{\mathrm{VBF}}^{h_i}(X) \equiv (C_{WW}^{h_i})^2 \frac{\mathrm{BR}(h_i \to X)}{\mathrm{BR}(h_{\mathrm{SM}} \to X)}, \tag{5}$$

where h_{SM} is the SM Higgs boson with $m_{h_{\mathrm{SM}}} = m_{h_i}$ and $C_{gg}^{h_i}, C_{WW}^{h_i}$ are the ratios of the $gg \to h_i$, $WW \to h_i$ couplings (C_{WW}^A being zero at tree level) to those for the SM, respectively. Note that the corresponding ratio for $V^* \to V h_i$ ($V = W, Z$) with $h_i \to X$ is equal to $R_{\mathrm{VBF}}^{h_i}(X)$, given that kinematic factors cancel out of all these ratios and that these ratios are computed in a self-consistent manner (that is, treating radiative corrections for the SM Higgs boson in the same manner as for the 2HDM Higgs bosons). When considering cases where more than one h_i has mass of 125 GeV [6], we sum the different R^{h_i} for the production/decay channel of interest.

We have performed five scans over the parameter space with the range of variation specified in Table II.

	scenario I	scenario II	scenario III	scenario IV	scenario V
m_h [GeV]	125	{10,..., 124.9}	125	125	{10,..., 124.9}
m_H [GeV]	125+{0.1,...,1000}	125	125.1	125+{0.1,...,1000}	125
m_A [GeV]	{10,...,1000}	{10,...,1000}	{10,...,1000}	125.1	125.1
$m_{H^\pm}$ [GeV]	1500 ($\tan\beta$=0.5); 800 ($\tan\beta$=1); 250,350 ($\tan\beta$=2); 90,150,250,350 ($\tan\beta > 2$) for Type I 600 ($\tan\beta$=0.5); 500 ($\tan\beta$=1); 340 ($\tan\beta = 2$); 320 ($\tan\beta > 2$) for Type II				
$\tan\beta$	{0.5, ..., 20}				
$\sin\alpha$	{-1, ...,1}				
m_{12}^2 [GeV^2]	$\{-1000^2, \ldots, 1000^2\}$				

TABLE II: Range of parameters adopted in the scans. The values of $m_{H^\pm}$ are bounded from below by the constraints from B physics, see Fig. 15 and Fig. 18 of [12] for the Type II and Type I models, respectively.

[1] We have modified the subroutine in 2HDMC that calculates the Higgs boson decays to $\gamma\gamma$ and also the part of the code relevant for QCD corrections to the $q\bar{q}$ final state.

A. The $m_h = 125$ GeV or $m_H = 125$ GeV scenarios:

Let us begin by discussing the case in which the h has mass $m_h = 125$ GeV while scanning over the masses of the other Higgs eigenstates (degenerate cases are discussed below). In Fig. 1, we plot the maximum value achieved for the ratio $R^h_{gg}(\gamma\gamma)$ as a function of $\tan\beta$ after scanning over all other input parameters (as specified earlier), in particular $\sin\alpha$. These maximum values are plotted prior to imposing any constraints and after imposing various combinations of the constraints outlined earlier with point notation as specified in the figure legend. We observe that for most

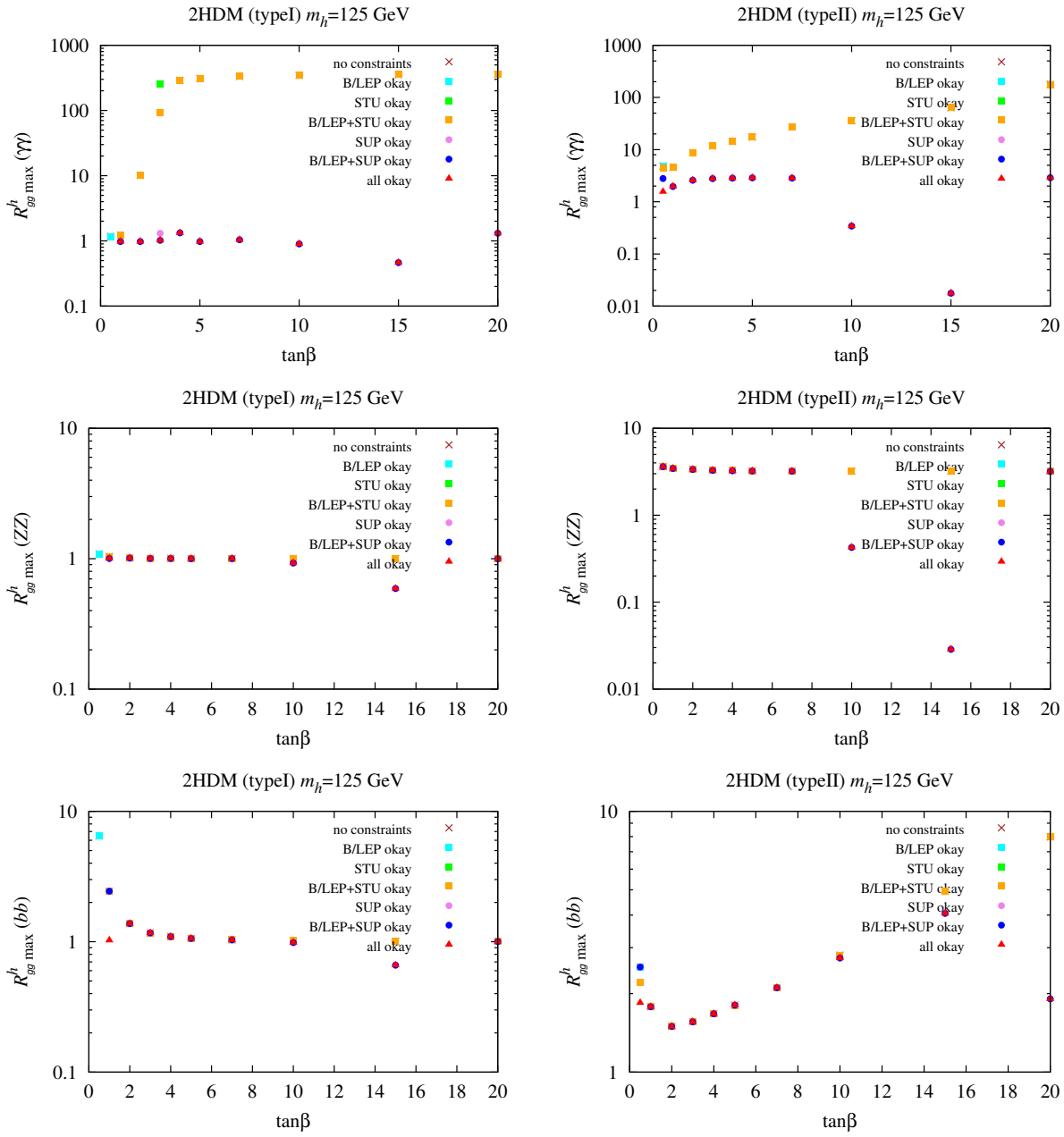

FIG. 1: The top two plots show the maximum $R^h_{gg}(\gamma\gamma)$ values in the Type I (left) and Type II (right) models for $m_h = 125$ GeV as a function of $\tan\beta$ after imposing various constraints — see figure legend. Corresponding $R^h_{gg}(ZZ)$ and $R^h_{gg}(bb)$ are shown in the middle and lower panels. Disappearance of a point after imposing a given constraint set means that the point did not satisfy that set of constraints. In the case of boxes and circles, if a given point satisfies subsequent constraints then the resulting color is chosen according to the color ordering shown in the legend, the same pattern is adopted in the remaining plots.

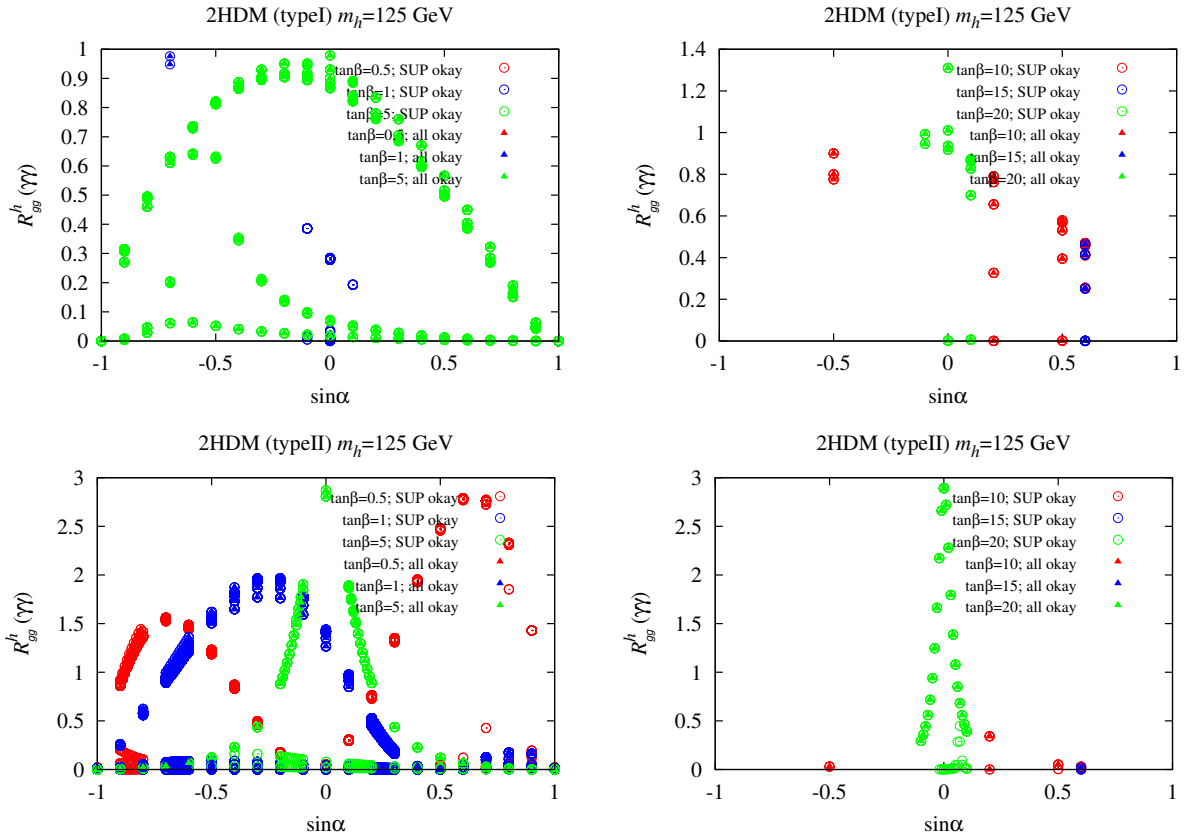

FIG. 2: $R^h_{gg}(\gamma\gamma)$ is plotted for $m_h = 125$ GeV as a function of $\sin\alpha$ for a sequence of $\tan\beta$ values. Different constraint combinations are considered and the different curves of given type correspond to a variety of other input parameters. The upper plots are for the Type I model and the lower plots are for the Type II model. Different colors indicate different $\tan\beta$ values.

values of $\tan\beta$ the B/LEP and STU precision electroweak constraints, both individually and in combination, leave the maximum $R^h_{gg}(\gamma\gamma)$ unchanged relative to a full scan over all of parameter space. In contrast, the SUP constraints greatly reduce the maximum value of $R^h_{gg}(\gamma\gamma)$ that can be achieved and that value is left unchanged when B/LEP and STU constraints are imposed in addition. Remarkably, in the Type I model maximum $R^h_{gg}(\gamma\gamma)$ values much above 1.3 are not possible, with values close to 1 being more typical for most $\tan\beta$ values, whereas maximum $R^h_{gg}(\gamma\gamma)$ values in the range of $2-3$ are possible for $2 \leq \tan\beta \leq 7$ and $\tan\beta = 20$ in the Type II model.

One can get a feeling for how the different constraints impact $R^h_{gg}(\gamma\gamma)$ by plotting this quantity as a function of $\sin\alpha$ at fixed $\tan\beta$ for different constraint combinations and a selection of different other input parameters. As shown in Fig. 2, $R^h_{gg}(\gamma\gamma)$ typically has a maximum as $\sin\alpha$ is varied but the height of this maximum depends very much on the constraints imposed as there is also variation with the other input parameters.

Tables III and IV display the full set of input parameters corresponding to the maximal $R^h_{gg}(\gamma\gamma)$ values at each $\tan\beta$ for models of Type I and Type II, respectively. It is important to notice that in the Type II model, the value of $R^h_{gg}(ZZ)$ corresponding to the parameters that maximize $R^h_{gg}(\gamma\gamma)$ is typically large, ~ 3. In fact, as discussed shortly, $R^h_{gg}(ZZ) > R^h_{gg}(\gamma\gamma)$ whenever $R^h_{gg}(\gamma\gamma)$ is even modestly enhanced. Since, experimentally, the observed signal for ZZ is substantially less enhanced than that for $\gamma\gamma$, the Type II models seem to be disfavored. We note that, in contrast, $R^h_{gg}(\gamma\gamma)/R^h_{gg}(ZZ) \gtrsim 1$ when $R^h_{gg}(\gamma\gamma) > 1$ is fairly typical of the MSSM model (which has a Type II Higgs sector), especially with full or partial GUT scale unification for the soft-SUSY-breaking parameters, see for example [17]. In such scenarios the primary modification to the $\gamma\gamma$ rate relative to the SM is due to the light stop loop contribution to the $h\gamma\gamma$ coupling (which enters with the same sign as the W loop and has a color factor enhancement) which enhances $\mathrm{BR}(h \to \gamma\gamma)$. Note that the stop loop contribution to the hgg production coupling is the same for both the ZZ and $\gamma\gamma$ final states. In the absence of GUT scale unification, there are many other potentially significant loops contributing to an increase in the $h\gamma\gamma$ coupling, the most important being the light chargino loop and the light stau

$\tan\beta$	$R^h_{gg\max}(\gamma\gamma)$	$R^h_{gg}(ZZ)$	$R^h_{gg}(b\bar{b})$	$R^h_{\rm VBF}(\gamma\gamma)$	$R^h_{\rm VBF}(ZZ)$	$R^h_{\rm VBF}(b\bar{b})$	m_H	m_A	$m_{H^\pm}$	m_{12}	$\sin\alpha$	$\mathcal{A}^h_{H^\pm}/\mathcal{A}$	δa_μ
1.0	0.98	1.00	1.02	0.96	0.98	1.00	875	750	800	500	-0.7	-0.01	-2.3
2.0	0.98	0.98	0.92	1.04	1.04	0.98	425	500	350	200	-0.5	-0.01	-1.8
3.0	1.02	0.98	0.92	1.08	1.04	0.98	225	400	150	100	-0.4	0.01	-1.7
4.0	1.33	0.99	1.07	1.24	0.93	0.99	225	200	90	100	-0.1	0.14	-1.7
5.0	0.98	0.98	1.06	0.90	0.91	0.98	225	400	150	100	-0.0	0.01	-1.6
7.0	1.04	0.99	0.98	1.06	1.01	0.99	135	500	90	50	-0.2	0.02	-1.6
10.0	0.90	0.81	0.74	0.99	0.89	0.81	175	500	150	50	-0.5	0.04	-1.5
15.0	0.46	0.59	0.66	0.41	0.53	0.59	225	400	350	50	0.6	-0.11	-1.4
20.0	1.31	1.00	1.00	1.30	0.99	1.00	225	200	90	50	-0.0	0.13	-1.5

TABLE III: Table of maximum $R^h_{gg}(\gamma\gamma)$ values for the Type I 2HDM with $m_h = 125$ GeV and associated R values for other initial and/or final states. The input parameters that give the maximal $R^h_{gg}(\gamma\gamma)$ value are also tabulated.

$\tan\beta$	$R^h_{gg\max}(\gamma\gamma)$	$R^h_{gg}(ZZ)$	$R^h_{gg}(b\bar{b})$	$R^h_{\rm VBF}(\gamma\gamma)$	$R^h_{\rm VBF}(ZZ)$	$R^h_{\rm VBF}(b\bar{b})$	m_H	m_A	$m_{H^\pm}$	m_{12}	$\sin\alpha$	$\mathcal{A}^h_{H^\pm}/\mathcal{A}$	δa_μ
0.5	1.56	2.69	1.84	0.52	0.89	0.61	425	500	600	100	-0.7	-0.06	-0.5
1.0	1.97	3.36	0.39	0.65	1.11	0.13	125	500	500	100	-0.2	-0.06	0.7
2.0	2.59	3.36	0.00	1.48	1.92	0.00	225	200	340	100	-0.0	-0.05	1.6
3.0	2.78	3.29	0.00	2.01	2.37	0.00	225	200	320	100	-0.0	-0.05	1.6
4.0	2.84	3.25	0.00	2.24	2.57	0.00	225	200	320	100	-0.0	-0.04	1.6
5.0	2.87	3.23	0.00	2.37	2.66	0.00	225	200	320	100	-0.0	-0.04	1.6
7.0	2.83	3.21	0.00	2.42	2.75	0.00	135	300	320	50	-0.0	-0.05	0.8
10.0	0.34	0.43	1.89	0.22	0.28	1.23	325	200	320	100	0.2	-0.08	3.5
15.0	0.02	0.03	4.06	0.00	0.01	0.87	225	200	320	50	0.6	-0.14	5.3
20.0	2.89	3.19	0.00	2.57	2.83	0.00	225	200	320	50	-0.0	-0.04	2.4

TABLE IV: Table of maximum $R^h_{gg}(\gamma\gamma)$ values for the Type II 2HDM with $m_h = 125$ GeV and associated R values for other initial and/or final states. The input parameters that give the maximal $R^h_{gg}(\gamma\gamma)$ value are also tabulated.

loop, as studied for example in [18].

Corresponding results for the H are presented for the Type I and Type II models in Tables V and VI, respectively. In the case of the Type I model, an enhanced gluon fusion rate in the $\gamma\gamma$ final state does not seem to be possible after imposing the SUP constraints, whereas maximal enhancements of order $R^H_{gg}(\gamma\gamma) \sim 2.8$ are quite typical for the Type II model, albeit with even larger $R^H_{gg}(ZZ)$. Again, in the case of the Type II model $R^H_{gg}(\gamma\gamma)/R^H_{gg}(ZZ) < 1$ applies more generally whenever $R^H_{gg}(\gamma\gamma)$ is significantly enhanced.

That an enhanced $\gamma\gamma$ rate, *e.g.* $R^{h,H}_{gg}(\gamma\gamma) > 1.2$, leads to $R^{h,H}_{gg}(\gamma\gamma)/R^{h,H}_{gg}(ZZ) < 1$ in Type II models is illustrated by the plots of Fig. 3. We again emphasize that this is to be contrasted with the Type I model for which $R^h_{gg}(\gamma\gamma) > 1.2$ implies $R^h_{gg}(\gamma\gamma)/R^{h,H}_{gg}(ZZ) > 1$, see Fig. 4, in better agreement with current data. (For the Type I model, $R^H_{gg}(\gamma\gamma) > 1$ is not possible after imposing the SUP constraints.)

It is interesting to understand the mechanism behind the enhancement of $R^{h,H}_{gg}(ZZ)$ that seems to be an inevitable result within the Type II model if $R^{h,H}_{gg}(\gamma\gamma)$ is large. Let us define r as the ratio of $\gamma\gamma$ over ZZ production rates for a scalar s (either h or H). Then it is easy to see that

$$r_s \equiv \frac{R^s_{gg}(\gamma\gamma)}{R^s_{gg}(ZZ)} = \frac{\Gamma(s\to\gamma\gamma)/\Gamma(h_{sm}\to\gamma\gamma)}{\Gamma(s\to ZZ)/\Gamma(h_{sm}\to ZZ)}\,. \tag{6}$$

For the decay mode $s \to ZZ^*$, the tree level amplitude is present and dominant so that the numerator simply reduces to $(C^s_{ZZ})^2$. For the decay mode $s \to \gamma\gamma$, there is no tree level contribution — the $s\gamma\gamma$ coupling first arises at the one-loop level with the t-loop, W-loop and $H^\pm$-loop being the important contributions. As a result, the denominator can be written as

$$\frac{\Gamma(s\to\gamma\gamma)}{\Gamma(h_{sm}\to\gamma\gamma)} = \left(\frac{C^s_{WW}\mathcal{A}^{SM}_W - C^s_{t\bar{t}}\mathcal{A}^{SM}_t + \mathcal{A}_{H^\pm}}{\mathcal{A}^{SM}_W - \mathcal{A}^{SM}_t}\right)^2 \tag{7}$$

where $C^s_{t\bar{t}}$ and C^s_{WW} are the $st\bar{t}$ and sWW couplings normalized to those of the $h_{\rm SM}$, while $\mathcal{A}^{SM}_W$ and $\mathcal{A}^{SM}_t$ are the W-loop and t-loop amplitudes, respectively, for the $h_{\rm SM}$. Finally, $\mathcal{A}_{H^\pm}$ is the $H^\pm$-loop amplitude in the 2HDM; since

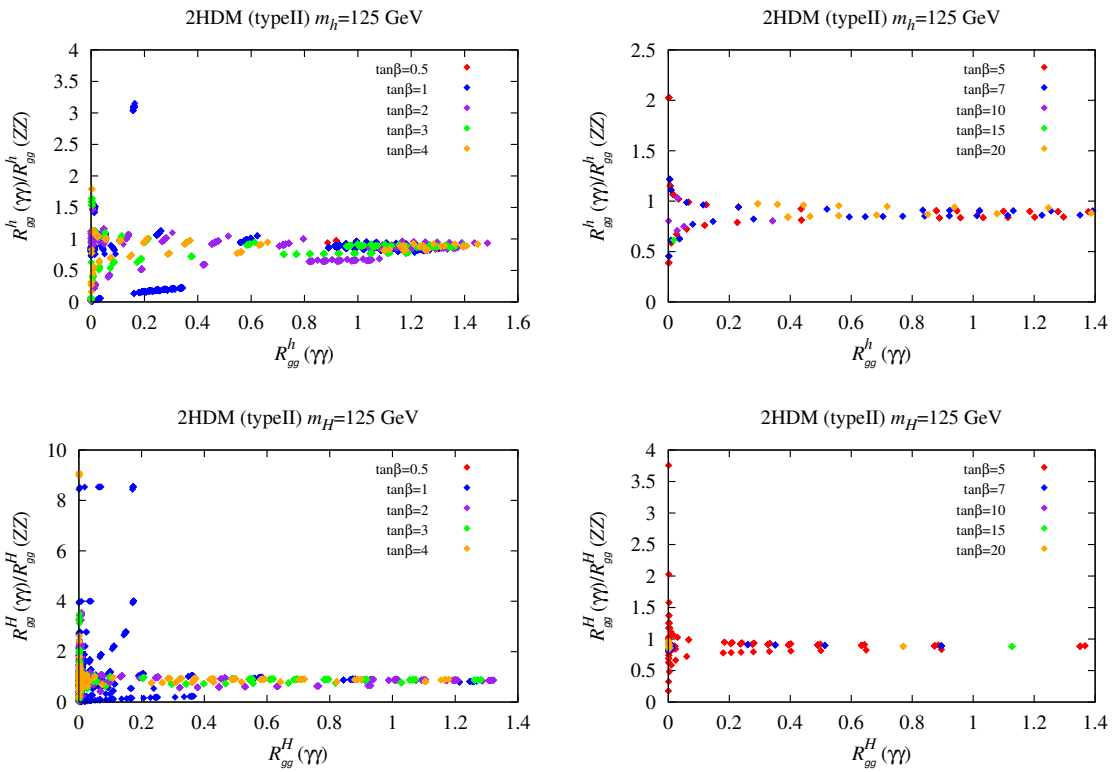

FIG. 3: For the h (top) and H (bottom) we plot the gluon fusion induced $\gamma\gamma/ZZ$ ratio as a function of $R_{gg}(\gamma\gamma)$ for the Type II 2HDM.

it is very small in the Type II model, it can be neglected. Thus,

$$r_s \simeq \frac{(C^s_{WW})^2}{(C^s_{ZZ})^2}\left(\frac{\mathcal{A}^{SM}_W - \frac{C^s_{t\bar{t}}}{C^s_{WW}}\mathcal{A}^{SM}_t}{\mathcal{A}^{SM}_W - \mathcal{A}^{SM}_t}\right)^2 = \left(\frac{\mathcal{A}^{SM}_W - \frac{C^s_{t\bar{t}}}{C^s_{WW}}\mathcal{A}^{SM}_t}{\mathcal{A}^{SM}_W - \mathcal{A}^{SM}_t}\right)^2 \tag{8}$$

where $C^s_{ZZ} = C^s_{WW}$ in any doublets+singlets models. Note that when the t-loop contribution is negligible then $r_s \to 1$. It is easy to see that $r_s < 1$ if the following inequality is satisfied

$$1 < \frac{C^s_{t\bar{t}}}{C^s_{WW}} < 2\frac{\mathcal{A}^{SM}_W}{\mathcal{A}^{SM}_t} - 1 \tag{9}$$

When $C^s_{t\bar{t}}/C^s_{WW}$ is outside of the above interval then $r_s > 1$. If s is the lighter scalar h then $C^s_{t\bar{t}}/C^s_{WW} = \cos\alpha/[\sin\beta\sin(\beta-\alpha)]$ implying $r_h < 1$ when

$$1 < \frac{\cos\alpha}{\sin\beta\sin(\beta-\alpha)} < 2\frac{\mathcal{A}^{SM}_W}{\mathcal{A}^{SM}_t} - 1 \simeq 9\,, \tag{10}$$

while for $s = H$, $C^s_{t\bar{t}}/C^s_{WW} = \sin\alpha/[\sin\beta\cos(\beta-\alpha)]$ and we obtain $r_H < 1$ for

$$1 < \frac{\sin\alpha}{\sin\beta\cos(\beta-\alpha)} < 2\frac{\mathcal{A}^{SM}_W}{\mathcal{A}^{SM}_t} - 1 \simeq 9. \tag{11}$$

In the case $s = h$, $R^h_{gg}(\gamma\gamma)$ is maximized by suppressing the h total width, which corresponds to chosing α so as to minimize the $hb\bar{b}$ coupling, *i.e.* $\alpha \sim 0$, resulting in $C^h_{t\bar{t}}/C^h_{WW} \sim 1/\sin^2\beta > 1$ (and < 5 for $\tan\beta > 0.5$). Consequently $r_h < 1$, as observed in Table IV. The argument is similar in the case of the H: this time the $Hb\bar{b}$ coupling is chosen to

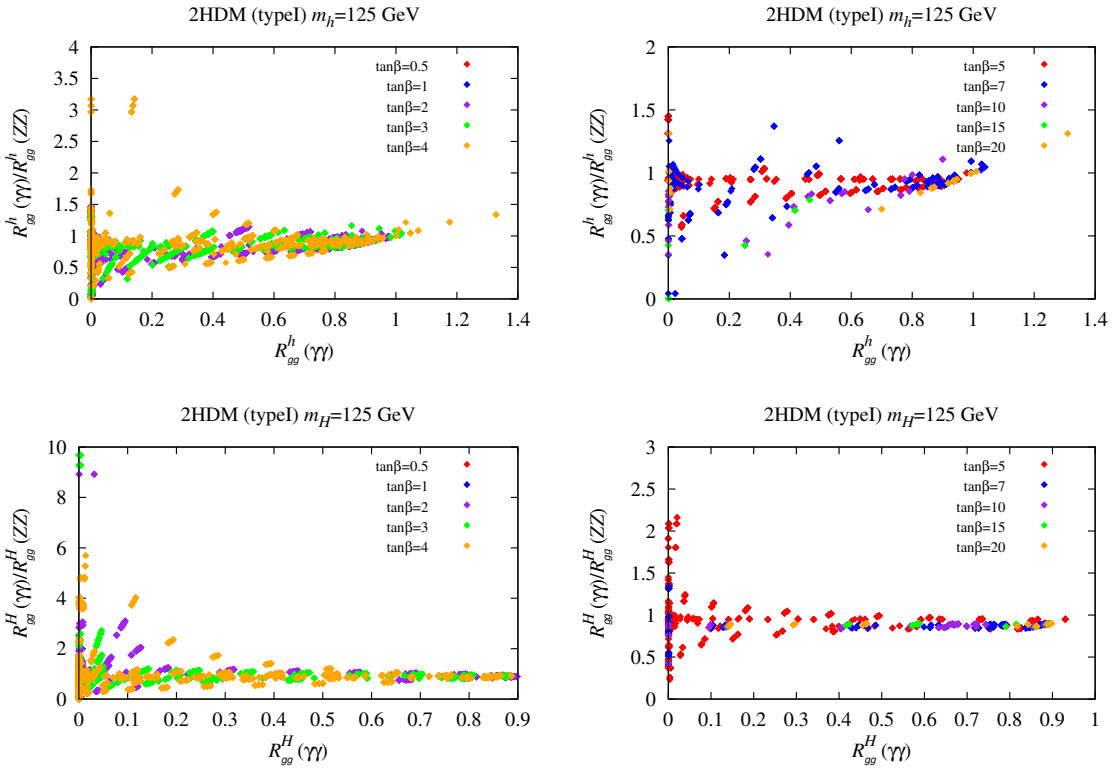

FIG. 4: For the h (top) and H (bottom) we plot the gluon fusion induced $\gamma\gamma/ZZ$ ratio as a function of $R_{gg}(\gamma\gamma)$ for the Type I 2HDMl.

be small (equivalent to $\alpha \sim \pm\pi/2$) in order to minimize the H total width and therefore maximize $R^H_{gg}(\gamma\gamma)$, with the result that once again $C^H_{t\bar{t}}/C^H_{WW} \sim 1/\sin^2\beta > 1$, yielding $r_H < 1$. These analytic results explain why large $R^s_{gg}(\gamma\gamma)$ is correlated with even larger $R^s_{gg}(ZZ)$ in Type II 2HDMs.

In Fig. 5 we plot contours of r_s and of $R^s_{gg}(\gamma\gamma)$ in the Type II model. It is seen from the left panel that if $\tan\beta$ is large then only small α's will maximize $R^s_{gg}(\gamma\gamma)$. And, in that region, r_h is always less than 1. Note that the $R^s_{gg}(\gamma\gamma) > 1$ region shrinks for large $\tan\beta$, so the the values of α preferred for large $R^h_{gg}(\gamma\gamma)$ converge to 0 when $\beta \to \pi/2$. For the case of $s = H$, the right panel shows that when $\tan\beta$ is large then only vertical bands of α corresponding to values close to $\pm\pi/2$ are allowed if $R^s_{gg}(\gamma\gamma) > 1$. From the plots, we see that $R^s_{gg}(\gamma\gamma) > 1$ could be consistent with $r_s > 1$ only if $\tan\beta \lesssim 1$, which explains the pattern observed in Tables IV and VI and Fig.3. Note, however, that small $\tan\beta$ is disfavored by B-physics as it enhances the $H^+\bar{t}b$ coupling too much, see for example [12].

Once again, we emphasize that a substantial enhancement of the $\gamma\gamma$ rate *is* possible for the h in Type I models without enhancing the ZZ rate. In particular, from Table III we see that the enhancement in the $\gamma\gamma$ channel is ~ 1.3 (for both gg fusion and VBF) for $\tan\beta = 4$ and 20 while other final states, in particular ZZ, have close to SM rates. The table also shows that this maximum is achieved for $\sin\alpha \sim 0$. Thus, $\beta \sim \pi/2$ and $\cos\alpha \sim 1$ yielding SM-like coupling of the h to quarks (see Table I) and vector bosons. It turns out that in these cases the total enhancement, $\sim 30\%$, is provided by the charged Higgs boson loop contribution to the $\gamma\gamma$-coupling. In these same cases, the mass of the heavier Higgs boson is $m_H = 225$ GeV. As such a mass is within the reach of the LHC, it is important to make sure that the H cannot be detected (at least with the current data set). It is easy to see that indeed this is the case. Since $g_{HZZ} \propto \cos(\beta-\alpha)$ and $g_{Hb\bar{b},Ht\bar{t}} \propto \sin\alpha$ one finds that the H decouples from both vector bosons and fermions given that $\alpha \sim 0$ and $\beta \sim \pi/2$. The A will also be difficult to detect since it has no tree-level WW, ZZ coupling and the $Ab\bar{b}, At\bar{t}$ couplings, being proportional to $\cot\beta$, will be quite suppressed, especially at $\tan\beta = 20$. From Table III, we observe that for $\tan\beta = 4$ and 20 the corresponding charged Higgs is light, $m_{H^\pm} = 90$ GeV, *i.e.* as small as allowed by LEP2 direct searches in $e^+e^- \to H^+H^-$. Searches for a light $H^\pm$ are underway at the LHC along the lines described in [19]. The most promising $H^\pm$ production and decay process is $pp \to t\bar{t} \to H^\pm bW^\mp\bar{b} \to \tau\nu b\bar{b}q'\bar{q}$. According to Fig. 3 of [19], for the Type I model, the region of $\tan\beta \lesssim 6-7$ for $m_{H^\pm} \sim 90$ GeV could be efficiently explored at the 14 TeV

$\tan\beta$	$R^H_{gg\max}(\gamma\gamma)$	$R^H_{gg}(ZZ)$	$R^H_{gg}(b\bar{b})$	$R^H_{\rm VBF}(\gamma\gamma)$	$R^H_{\rm VBF}(ZZ)$	$R^H_{\rm VBF}(b\bar{b})$	m_h	m_A	$m_{H^\pm}$	m_{12}	$\sin\alpha$	$\mathcal{A}^H_{H^\pm}/\mathcal{A}$	δa_μ
2.0	0.90	1.00	1.02	0.89	0.99	1.00	125	400	350	50	0.9	-0.05	-2.1
3.0	0.89	0.96	0.88	0.97	1.05	0.96	125	400	350	50	0.9	-0.05	-1.8
4.0	0.89	0.97	1.09	0.79	0.86	0.97	105	500	90	50	1.0	-0.03	-1.7
5.0	0.93	0.98	1.06	0.86	0.90	0.98	125	500	90	50	1.0	-0.01	-1.6
7.0	0.88	0.99	1.03	0.85	0.95	0.99	65	400	350	10	1.0	-0.05	-1.6
10.0	0.89	1.00	1.02	0.87	0.98	1.00	45	400	350	0	1.0	-0.05	-1.6
15.0	0.90	1.00	1.01	0.89	0.99	1.00	5	400	350	0	-1.0	-0.05	-1.6
20.0	0.90	1.00	1.00	0.89	0.99	1.00	25	400	350	0	-1.0	-0.05	-1.5

TABLE V: Table of maximum $R^H_{gg}(\gamma\gamma)$ values for the Type I 2HDM with $m_H = 125$ GeV and associated R values for other initial and/or final states. The input parameters that give the maximal $R^H_{gg}(\gamma\gamma)$ value are also tabulated.

$\tan\beta$	$R^H_{gg\max}(\gamma\gamma)$	$R^H_{gg}(ZZ)$	$R^H_{gg}(b\bar{b})$	$R^H_{\rm VBF}(\gamma\gamma)$	$R^H_{\rm VBF}(ZZ)$	$R^H_{\rm VBF}(b\bar{b})$	m_h	m_A	$m_{H^\pm}$	m_{12}	$\sin\alpha$	$\mathcal{A}^H_{H^\pm}/\mathcal{A}$	δa_μ
1.0	1.99	3.24	0.52	0.71	1.16	0.19	125	500	500	100	1.0	-0.06	0.7
2.0	2.56	3.36	0.00	1.46	1.92	0.00	125	300	340	50	1.0	-0.06	1.1
3.0	2.73	3.29	0.00	1.97	2.37	0.00	125	300	320	50	1.0	-0.05	1.0
4.0	2.78	3.25	0.00	2.20	2.57	0.00	125	300	320	50	-1.0	-0.05	1.0
5.0	2.81	3.23	0.00	2.32	2.66	0.00	125	300	320	50	-1.0	-0.05	0.9
7.0	2.80	3.21	0.00	2.40	2.75	0.00	65	300	320	10	-1.0	-0.06	-0.0
10.0	2.81	3.20	0.00	2.46	2.79	0.00	45	300	320	0	-1.0	-0.06	-2.8
15.0	2.82	3.19	0.00	2.49	2.82	0.00	25	300	320	0	-1.0	-0.05	-16.9
20.0	2.82	3.19	0.00	2.50	2.83	0.00	25	300	320	0	-1.0	-0.05	-30.8

TABLE VI: Table of maximum $R^H_{gg}(\gamma\gamma)$ values for the Type II 2HDM with $m_H = 125$ GeV and associated R values for other initial and/or final states. The input parameters that give the maximal $R^H_{gg}(\gamma\gamma)$ value are also tabulated.

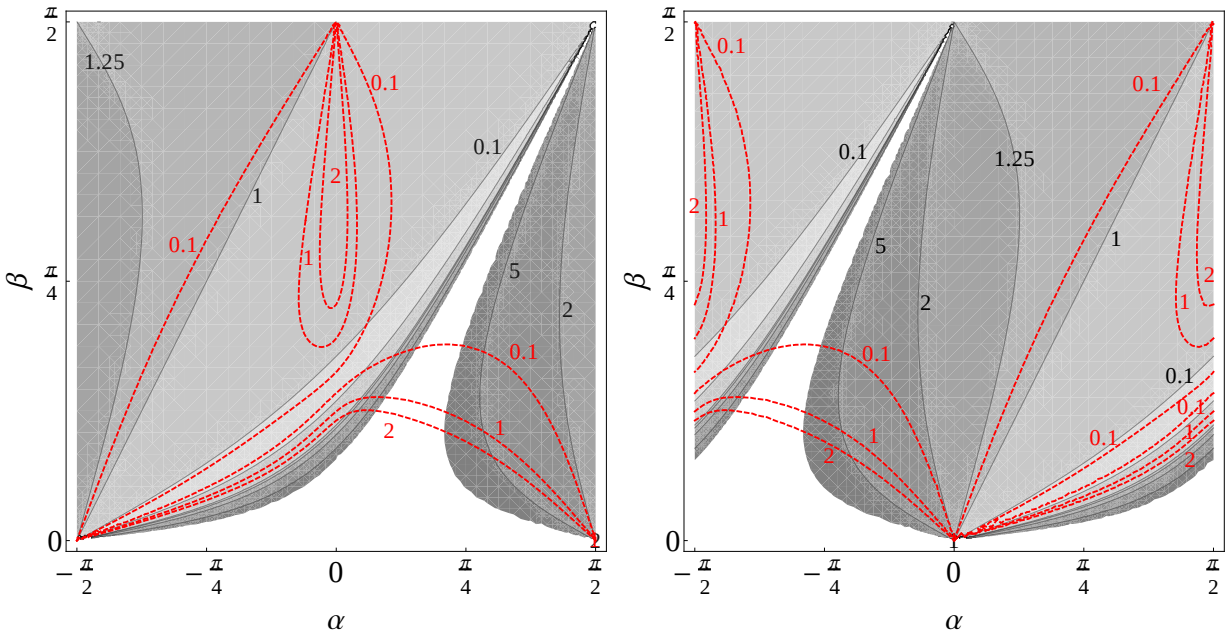

FIG. 5: In the left panel we show contour plots (with shadowing) in the (β, α) space for r_h with superimposed red contours for $R^h_{gg}(\gamma\gamma)$. The right panel show similarly r_H with $R^H_{gg}(\gamma\gamma)$. Red numbers give constant values of $R^h_{gg}(\gamma\gamma)$ ($R^H_{gg}(\gamma\gamma)$) while black ones show constant values of r_h (r_H). The white region correspond to $r_s > 10.75$.

LHC by ATLAS even at the integrated luminosity of 10 fb^{-1} – for more details see [19]. The existing LHC bounds on $BR(t \to H^+b)$ obtained assuming BR$(H^\pm \to \tau^\pm\nu_\tau) = 1$ are only moderately restrictive: $5\% - 1\%$ [20] $(4\% - 2\%)$[21] for masses of the charged Higgs boson $m_{H^\pm} = 90(80) - 160$ GeV in the case of ATLAS (CMS), respectively. These bounds are weakened in the Type I model where $BR(H^\pm \to \tau^\pm\nu_\tau) \simeq 0.7$. Since $BR(t \to H^+b) \sim 1/\tan^2\beta$, large $\tan\beta$ suppresses $BR(t \to H^+b)$. Indeed, it is easy to verify that for $m_{H^\pm} = 90$ GeV $BR(t \to H^+b)$ is $\sim 3.8\%$ and $\sim 0.15\%$ for $\tan\beta = 4$ and $\tan\beta = 20$, respectively. So, a charged Higgs yielding enhanced $h \to \gamma\gamma$ rates in gg fusion

and VBF is still completely consistent with current data.

B. $m_A \sim 125$ GeV and $m_h = 125$ GeV or $m_H = 125$ GeV scenario

The signal at 125 GeV cannot be pure A since the A does not couple to ZZ, a final state that is definitely present at 125 GeV. However, one can imagine that the $\mathcal{CP}$-even h or H and the A both have mass of 125 GeV and that the net $\gamma\gamma$ rate gets substantial contributions from both the h or H and the A while only the former contributes to the ZZ rate. These possibilities are explored in Figs. 6 and 7, from which we observe that an enhanced $\gamma\gamma$ rate is only possible for the $m_h = m_A = 125$ GeV choice. Details for this case appear in Table VII.

For the Type I model, we see from Table VII that $R^h_{gg}(\gamma\gamma)$ is significantly enhanced only for the same $\tan\beta = 4$ and $\tan\beta = 20$ values as in the case of having (only) $m_h = 125$ GeV and that the pseudoscalar contribution $R^A_{gg}(\gamma\gamma)$ turns out to be tiny. However, the contribution to the $b\bar{b}$ final state from the A *can* be substantial. Given that the top loop dominates both the Agg and hgg coupling one finds $(C^A_{gg}/C^h_{gg})^2 \sim (3/2)^2(\cos\beta/\cos\alpha)^2$, where we used $C^A_{t\bar{t}}/C^h_{t\bar{t}} = \cos\beta/\cos\alpha$ from Table I and the $m_{h,A} \ll 2m_t$ fermionic loop ratio of $A/h = 3/2$. As a result, the A can contribute even more to the $b\bar{b}$ final state rate than the h if $\tan\beta$ is small. This (unwanted) contribution to the $b\bar{b}$ final state from A production is apparent from the results for $R^{h+A}_{gg}(b\bar{b})$ in Table VII for $\tan\beta = 2-4$. In the end, only $\tan\beta = 20$ yields both an enhanced $\gamma\gamma$ rate, $R^{h+A}_{gg\,\max}(\gamma\gamma) = 1.31$, and SM-like rates for the ZZ and $b\bar{b}$ final states, $R^{h+A}_{gg}(ZZ) = R^{h+A}_{gg}(b\bar{b}) = 1$. For this case $\beta \simeq \pi/2$ and $\alpha = 0$ implying that the h couples to fermions and gauge bosons like a SM Higgs boson and the enhancement of $R^{h+A}_{gg\,\max}(\gamma\gamma)$ is due exclusively to the charged Higgs loop contribution to the $\gamma\gamma$ couplings.

For the Type II model, see Table VIII, the pseudoscalar contribution $R^A_{gg}(\gamma\gamma)$ is also (as for the Type I model) negligible. Thus, the enhancement of $R^{h+A}_{gg}(\gamma\gamma)$ is essentially the same as that for $R^h_{gg}(\gamma\gamma)$ for the case when only $m_h = 125$ GeV, reaching maximum values of order $2-3$. However, as in the pure $m_h = 125$ GeV case, a substantial enhancement of $R^{h+A}_{gg}(\gamma\gamma)$ is most often associated with $R^{h+A}_{gg}(ZZ) > R^{h+A}_{gg}(\gamma\gamma)$ (contrary to the LHC observations). But this is not *always* the case. Among the $m_h = m_A$ scenarios we find 56 points in our parameter space for which $R^{h+A}_{gg}(ZZ) < 1.3$ and $R^{h+A}_{gg}(\gamma\gamma) > 1.3$. Unfortunately for all those points the $b\bar{b}$ signal is predicted to be too strong, $R^{h+A}_{gg}(b\bar{b}) > 3.82$. This situation is illustrated in Fig. 8. As seen from the upper panels in Fig. 8, for $\tan\beta = 1$ there exist points (blue diamonds) such that $r_h > 1$ and $R^{h+A}_{gg}(\gamma\gamma) > 1$ (or even > 1.5). However, the lower left panel of Fig. 8 shows that the $R^{h+A}_{gg}(b\bar{b})$ values that correspond to those points are greater than 3.5, a result that is disfavored

$\tan\beta$	$R^{h+A}_{gg\max}(\gamma\gamma)$	$R^h_{gg}(\gamma\gamma)$	$R^A_{gg}(\gamma\gamma)$	$R^{h+A}_{gg}(ZZ)$	$R^{h+A}_{gg}(b\bar{b})$	$R^h_{\rm VBF}(\gamma\gamma)$	$R^h_{\rm VBF}(ZZ)$	$R^h_{\rm VBF}(b\bar{b})$	m_H	$m_{H^\pm}$	m_{12}	$\sin\alpha$	$\mathcal{A}^h_{H^\pm}/\mathcal{A}$	δa_μ
2.0	1.07	0.92	0.15	0.98	1.73	0.98	1.04	0.98	325	250	100	-0.5	-0.04	-2.2
3.0	1.08	1.02	0.07	0.98	1.28	1.08	1.04	0.98	225	150	100	-0.4	0.01	-1.9
4.0	1.35	1.33	0.03	0.99	1.21	1.24	0.93	0.99	225	90	100	-0.1	0.14	-1.8
5.0	0.96	0.95	0.01	1.00	1.07	0.95	1.00	1.00	135	90	50	-0.2	-0.03	-1.7
7.0	1.04	1.04	0.01	0.99	1.00	1.06	1.01	0.99	135	90	50	-0.2	0.02	-1.6
10.0	0.91	0.90	0.01	0.81	0.77	0.99	0.89	0.81	175	150	50	-0.5	0.04	-1.5
15.0	0.42	0.42	0.00	0.59	0.67	0.37	0.53	0.59	225	250	50	0.6	-0.17	-1.4
20.0	1.31	1.31	0.00	1.00	1.00	1.30	0.99	1.00	225	90	50	-0.0	0.13	-1.6

TABLE VII: Table of maximum $R^{h+A}_{gg}(\gamma\gamma)$ values for the Type I 2HDM with $m_h = m_A = 125$ GeV and associated R values for other initial and/or final states. The input parameters that give the maximal $R^{h+A}_{gg}(\gamma\gamma)$ value are also tabulated.

$\tan\beta$	$R^{h+A}_{gg\max}(\gamma\gamma)$	$R^h_{gg}(\gamma\gamma)$	$R^A_{gg}(\gamma\gamma)$	$R^{h+A}_{gg}(ZZ)$	$R^{h+A}_{gg}(b\bar{b})$	$R^h_{\rm VBF}(\gamma\gamma)$	$R^h_{\rm VBF}(ZZ)$	$R^h_{\rm VBF}(b\bar{b})$	m_H	$m_{H^\pm}$	m_{12}	$\sin\alpha$	$\mathcal{A}^h_{H^\pm}/\mathcal{A}$	δa_μ
1.0	2.05	1.58	0.47	2.05	3.91	0.93	1.22	0.65	525	500	100	-0.5	-0.06	1.3
2.0	1.18	1.17	0.01	1.31	1.68	1.07	1.20	0.87	325	340	100	-0.4	-0.05	1.5
3.0	2.78	2.78	0.00	3.29	0.27	2.01	2.37	0.00	225	320	100	-0.0	-0.05	2.3
4.0	2.84	2.84	0.00	3.25	0.23	2.24	2.57	0.00	225	320	100	-0.0	-0.04	2.3
5.0	1.89	1.89	0.00	2.19	0.95	1.41	1.64	0.47	225	320	100	0.1	-0.05	2.7
7.0	0.04	0.04	0.00	0.06	2.85	0.01	0.02	0.75	325	320	100	0.6	-0.15	5.2
10.0	0.34	0.34	0.00	0.43	3.66	0.22	0.28	1.23	325	320	100	0.2	-0.08	4.7
20.0	2.89	2.89	0.00	3.19	8.03	2.57	2.83	0.00	225	320	50	-0.0	-0.04	5.6

TABLE VIII: Table of maximum $R^{h+A}_{gg}(\gamma\gamma)$ values for the Type II 2HDM with $m_h = m_A = 125$ GeV and associated R values for other initial and/or final states. The input parameters that give the maximal $R^{h+A}_{gg}(\gamma\gamma)$ value are also tabulated.

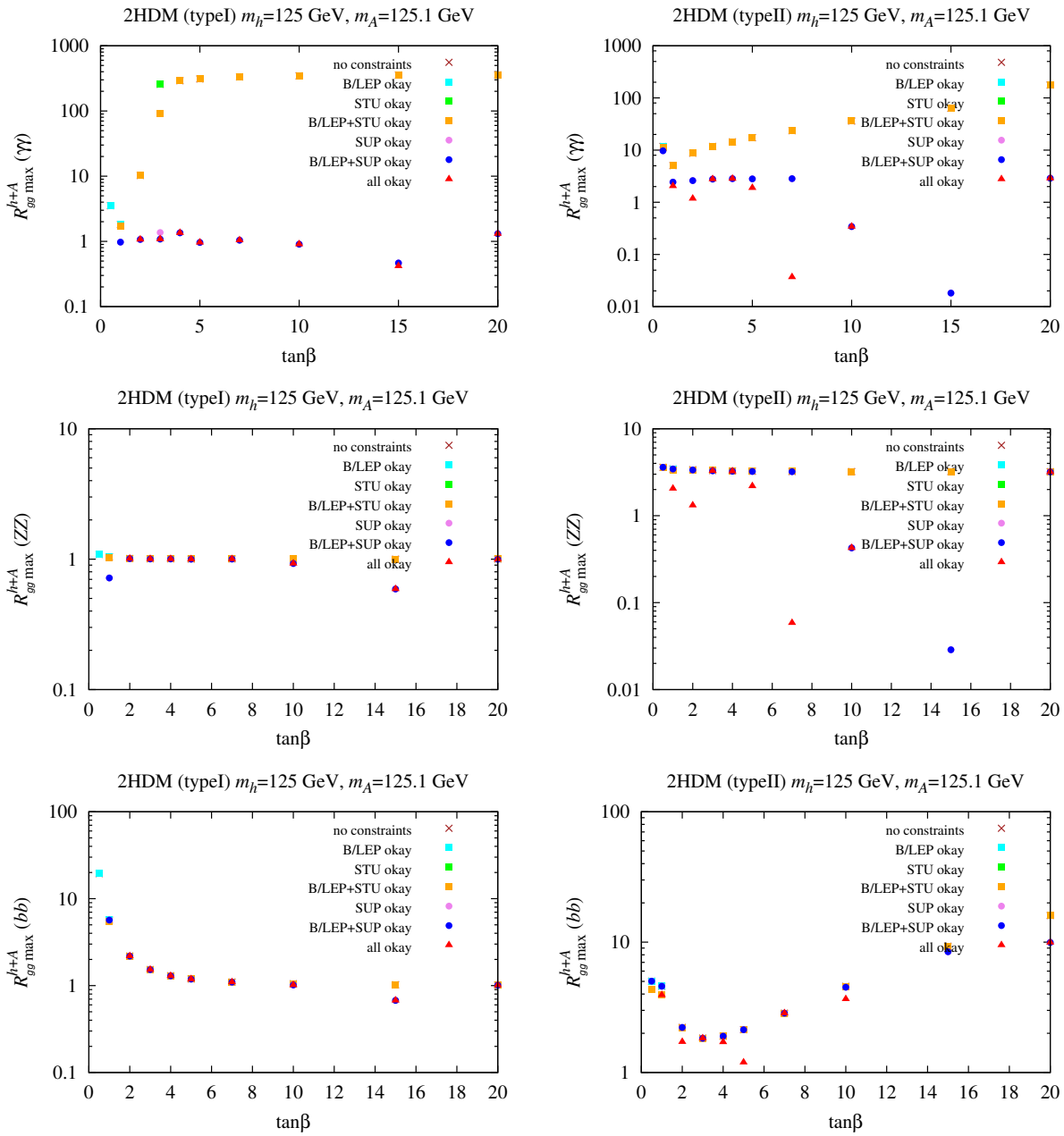

FIG. 6: $R^{h+A}_{gg}(\gamma\gamma)$ maximum values when $m_h = m_A = 125$ GeV as a function of $\tan\beta$ after imposing various constraints — see figure legend. Corresponding $R^{h}_{gg}(ZZ)$ and $R^{h}_{gg}(b\bar{b})$ are shown in the middle and lower panels.

by the LHC data.

The case with $m_A \sim 125$ GeV and $m_H = 125$ GeV is less attractive. For the Type I model, the constraints are such that once parameters are chosen so that H and A have the same mass of 125 GeV the maximum value achieved for $R^{H+A}_{gg\,\max}(\gamma\gamma)$ is rather modest reaching only 1.04 at small $\tan\beta$. For the Type II model, as seen in Fig. 7, there are no parameter choices for which the H and A have a mass of 125 GeV while all other constraints are satisfied.

C. $m_h = 125$ GeV and $m_H = 125$ GeV scenario

Finally, we have the case where the h and H have a common mass of 125 GeV and we allow $m_{H^\pm}$ and m_A to vary freely. Following a similar search strategy, we find that some of the previously available $\tan\beta$ values are ruled out by

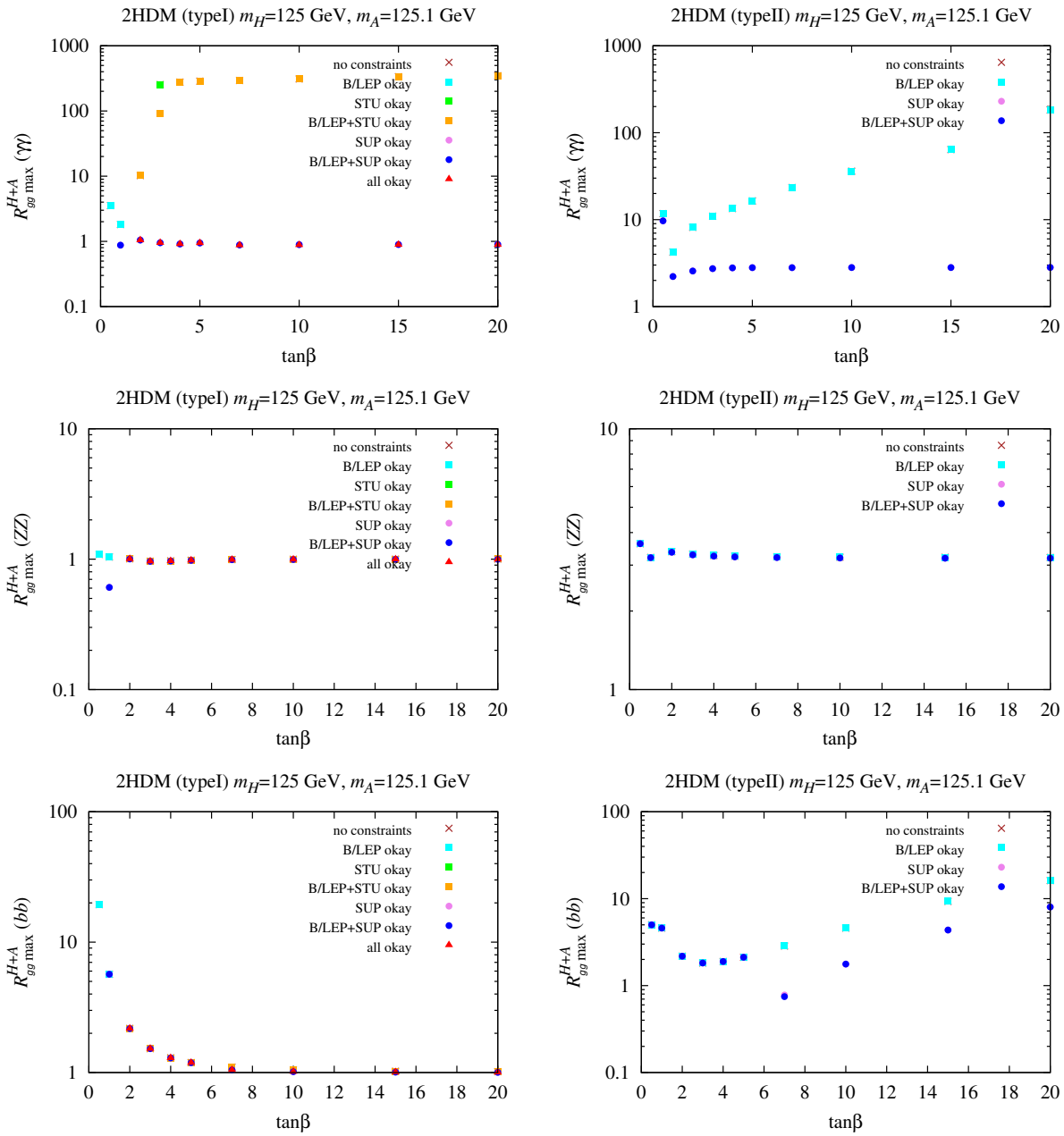

FIG. 7: As in Fig. 6 but for $m_H = m_A = 125$ GeV.

the full set of constraints and that there is no gain in maximal $R^{h+H}_{gg}(\gamma\gamma)$ values, and often some loss, relative to the cases where only the h or only the H was required to have mass of 125 GeV.

As discusssed earlier, the charged Higgs contribution to the $\gamma\gamma$ coupling loops is sometimes relevant. Therefore, in Fig. 9 we show separately the fermionic loop, W loop and $H^\pm$ loop contributions normalized to the total amplitude for the most interesting cases of a Type I model with $m_h = 125$ GeV and with $m_h = m_A = 125$ GeV (left plots). One sees that the tan β values of 4 and 20 associated with $R^h_{gg}(\gamma\gamma) \sim 1.3$ are associated with large $A_{H^\pm}/A$. Indeed, in these two cases, the relative charged Higgs contribution reaches nearly ~ 0.2 and is as large as the fermionic contribution, but of the opposite sign. In fact, although the dominant loop is the W loop, the $H^\pm$ loop may contribute as much as the dominant (top quark) fermionic loop.

This should be contrasted with other cases, such as the Type II $m_h = 125$ GeV and $m_h = m_A = 125$ GeV cases

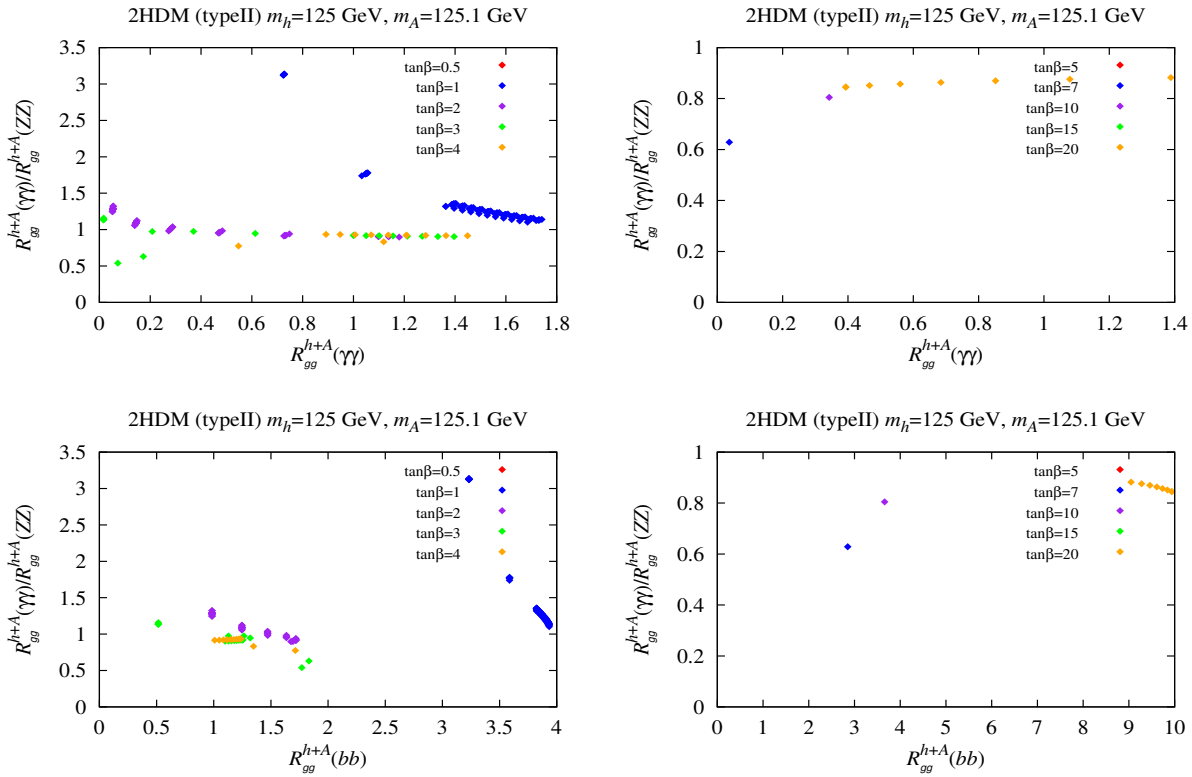

FIG. 8: Correlations between $R_{gg}^{h+A}(\gamma\gamma)/R_{gg}^{h+A}(ZZ)$ and $R_{gg}^{h+A}(\gamma\gamma)$ (upper panels) and $R_{gg}^{h+A}(b\bar{b})$ (lower panels) for selected values of $\tan\beta$.

illustrated in the right-hand plots of Fig. 9. One finds that the charged Higgs contributions are small when SUP constraints are imposed. In fact, the enhancement of $R_{gg}^{h}(\gamma\gamma)$ observed in Fig. 1 prior to imposing SUP is caused just by the charged Higgs loop. When SUP constraints are imposed the charged Higgs amplitude is strongly reduced by the requirement that the quartic couplings not violate the perturbativity condition. Note that the SUP constraints can be violated even though all the mass parameters have been varied within what, a priori, appears to be a reasonable range, namely from a few GeV up to 1000 GeV. This is due to the fact that, for our input, the SUP conditions imply a strong constraint on m_{12}^2 that comes mainly from the requirement of keeping λ_1 small enough.

IV. CONCLUSIONS

We have analyzed the Type I and Type II two-Higgs-doublet extensions of the Standard Model with regard to consistency with a significant enhancement of the gluon-fusion-induced $\gamma\gamma$ signal observed at the LHC at ~ 125 GeV. All possible theoretical and experimental constraints have been imposed. We find that vacuum stability, unitarity and perturbativity play the key role in limiting the maximal possible enhancement which, in the most interesting scenarios, is generated by the charged Higgs loop contribution to the Higgs to two photon decay amplitude. Generically, we conclude that the Type II model allows a maximal enhancement of order of $2-3$, whereas within the Type I model the maximal enhancement is limited to $\lesssim 1.3$. Current public results suggest an enhancement for $gg \to h \to \gamma\gamma$ that exceeds the maximum for the Type I model and would appear to favor the Type II model.

However, we find that in the Type II model the parameters that give $R_{gg}^{h}(\gamma\gamma) > 1.3$ are characterized by $R_{gg}^{h}(ZZ) > R_{gg}^{h}(\gamma\gamma)$, a result that is inconsistent with experimental results in the $gg \to h \to ZZ \to 4\ell$ channel. Thus, if $R_{gg}^{h}(\gamma\gamma) > 1.3$ and $R_{gg}^{h}(ZZ) < 1.3$ both persist experimentally, the Type II model cannot describe the data if only the h resides at 125 GeV. Similar statements apply to the case of the heavier H having a mass of 125 GeV. Next, we considered Type II models with approximately degenerate Higgs bosons at 125 GeV. We found that there exist theoretically consistent parameter choices for Type II models for which $R_{gg}^{h+A}(\gamma\gamma) > 1.3$ while $R_{gg}^{h+A}(ZZ) < 1.3$, but in these cases $R_{gg}^{h+A}(b\bar{b}) > 3.75$, a value far above that observed. Thus, the Type II 2HDMs cannot yield $R_{gg}^{h+A}(\gamma\gamma) > 1.3$

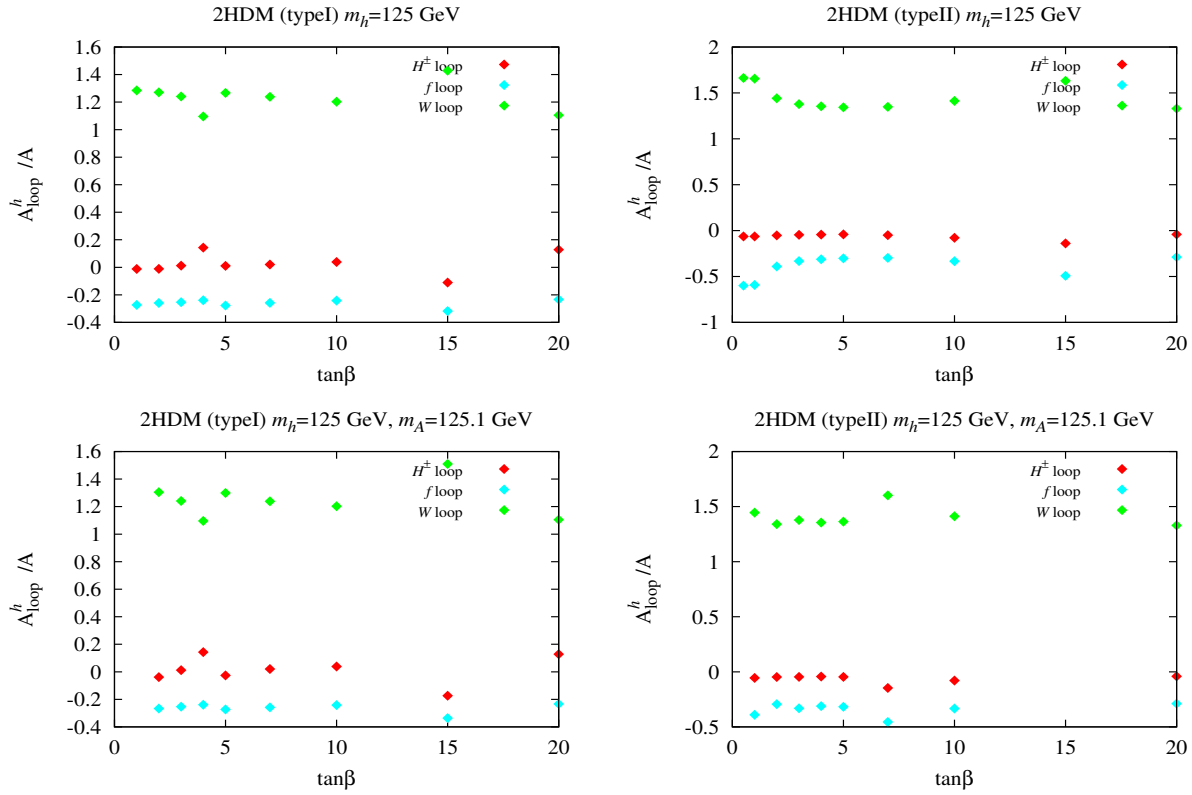

FIG. 9: For the most interesting scenarios we show imaginary part of charged Higgs contributions to the $\gamma\gamma$ amplitude normalized to the imaginary part of the sum of all (fermions, W^+W^-, H^+H^-) contributions as a function of $\tan\beta$ after imposing all constraints. The parameters adopted correspond to maximal $R^{h_i}_{gg}(\gamma\gamma)$ (or an appropriate sum for degenerate cases).

without conflicting with other observables. In short, the Type II model is unable to give a significantly enhanced $gg \to h \to \gamma\gamma$ signal while maintaining consistency with other channels.

In the case of the Type I model, the maximal $R^h_{gg}(\gamma\gamma)$ is of order of 1.3, as found if $\tan\beta = 4$ or 20. In these cases, $R^h_{gg}(ZZ)$ and $R^h_{gg}(b\bar{b})$ are of order 1 as fairly consistent with current data. For these scenarios, the charged Higgs is light, $m_{H^\pm} = 90$ GeV. Despite this small mass, there is no conflict with LHC data due to the fact that $BR(t \to H^+ b) \sim 1/\tan^2\beta$ is small enough to be below current limits. Thus, Type I models could provide a consistent picture if the LHC results converge to only a modest enhancement for $R^h_{gg}(\gamma\gamma) \lesssim 1.3$. But, if $R^h_{gg}(\gamma\gamma)$ is definitively measured to have a value much above 1.3 while the ZZ and $b\bar{b}$ channels show little enhancement then there is no consistent 2HDM description. One must go beyond the 2HDM to include new physics such as supersymmetry.

Acknowledgments

This work has been supported in part by US DOE grant DE-FG03-91ER40674 and by the National Science Centre (Poland) as a research project, decision no DEC-2011/01/B/ST2/00438. This work was supported by the Foundation for Polish Science International PhD Projects Programme co-financed by the EU European Regional Development Fund. JFG thanks the Galileo Galilei Institute for support during the completion of this work.

[1] G. Aad *et al.* [ATLAS Collaboration], Phys. Lett. B **716** (2012) 1 [arXiv:1207.7214 [hep-ex]].
[2] S. Chatrchyan *et al.* [CMS Collaboration], Phys. Lett. B **716**, 30 (2012) [arXiv:1207.7235 [hep-ex]].
[3] [TEVNPH (Tevatron New Phenomina and Higgs Working Group) and CDF and D0 Collaborations], arXiv:1203.3774 [hep-ex].
[4] P. M. Ferreira, R. Santos, M. Sher and J. P. Silva, Phys. Rev. D **85**, 035020 (2012) [arXiv:1201.0019 [hep-ph]].

[5] P. M. Ferreira, R. Santos, M. Sher and J. P. Silva, arXiv:1112.3277 [hep-ph].
[6] J. F. Gunion, Y. Jiang and S. Kraml, arXiv:1207.1545 [hep-ph].
[7] D. Eriksson, J. Rathsman and O. Stal, Comput. Phys. Commun. **181**, 833 (2010); D. Eriksson, J. Rathsman and O. Stal, Comput. Phys. Commun. **181**, 189 (2010) [arXiv:0902.0851 [hep-ph]].
[8] J. F. Gunion and H. E. Haber, Phys. Rev. D **67**, 075019 (2003) [hep-ph/0207010].
[9] J. F. Gunion, H. E. Haber, G. L. Kane and S. Dawson, Front. Phys. **80**, 1 (2000).
[10] G. Abbiendi *et al.* [OPAL Collaboration], Eur. Phys. J. C **27**, 311 (2003) [hep-ex/0206022].
[11] G. Abbiendi *et al.* [OPAL Collaboration], Eur. Phys. J. C **40**, 317 (2005) [hep-ex/0408097].
[12] G. C. Branco, P. M. Ferreira, L. Lavoura, M. N. Rebelo, M. Sher and J. P. Silva, Phys. Rept. **516**, 1 (2012) [arXiv:1106.0034 [hep-ph]].
[13] J. Beringer *et al.* [Particle Data Group Collaboration], Phys. Rev. D **86**, 010001 (2012).
[14] S. M. Barr and A. Zee, Phys. Rev. Lett. **65**, 21 (1990) [Erratum-ibid. **65**, 2920 (1990)].
[15] G. W. Bennett *et al.* [Muon g-2 Collaboration], Phys. Rev. Lett. **92**, 161802 (2004) [hep-ex/0401008].
[16] I. F. Ginzburg and I. P. Ivanov, Phys. Rev. D **72**, 115010 (2005) [hep-ph/0508020].
[17] F. Brummer, S. Kraml and S. Kulkarni, JHEP **1208**, 089 (2012) [arXiv:1204.5977 [hep-ph]].
[18] M. Carena, S. Gori, N. R. Shah, C. E. M. Wagner and L. -T. Wang, JHEP **1207**, 175 (2012) [arXiv:1205.5842 [hep-ph]].
[19] M. Aoki, R. Guedes, S. Kanemura, S. Moretti, R. Santos and K. Yagyu, Phys. Rev. D **84**, 055028 (2011) [arXiv:1104.3178 [hep-ph]].
[20] G. Aad *et al.* [ATLAS Collaboration], JHEP **1206**, 039 (2012) [arXiv:1204.2760 [hep-ex]].
[21] S. Chatrchyan *et al.* [CMS Collaboration], JHEP **1207**, 143 (2012) [arXiv:1205.5736 [hep-ex]].